Journal of Applied Physics

Solar-cell radiance standard for absolute electroluminescence measurements and open-circuit voltage mapping of silicon solar modules

Cite as: J. Appl. Phys. **119**, 034501 (2016); https://doi.org/10.1063/1.4940159
Submitted: 27 August 2015 • Accepted: 06 January 2016 • Published Online: 19 January 2016

Toshimitsu Mochizuki, Changsu Kim, Masahiro Yoshita, et al.

AIP Publishing

Solar-cell radiance standard for absolute electroluminescence measurements and open-circuit voltage mapping of silicon solar modules

Toshimitsu Mochizuki,[1,a)] Changsu Kim,[2,3] Masahiro Yoshita,[2,3] Jonathon Mitchell,[1] Zhu Lin,[2,3] Shaoqiang Chen,[3,4] Hidetaka Takato,[1] Yoshihiko Kanemitsu,[3,5] and Hidefumi Akiyama[2,3]

[1]*Fukushima Renewable Energy Institute, The National Institute of Advanced Industrial Science and Technology, Fukushima 963-0298, Japan*
[2]*Institute for Solid State Physics, The University of Tokyo, Chiba 277-8581, Japan*
[3]*JST-CREST, Tokyo 102-0076, Japan*
[4]*Department of Electronic Engineering, East China Normal University, Shanghai 200241, China*
[5]*Institute for Chemical Research, Kyoto University, Kyoto 611-0011, Japan*

(Received 27 August 2015; accepted 6 January 2016; published online 19 January 2016)

In this work, we propose and demonstrate a durable and distributable Lambertian light-emitter secondary standard using the electroluminescence (EL) of a Si solar cell. This standard is useful for calibration of the absolute sensitivity of an EL-imaging infrared camera used to acquire quick on-site measurements of the absolute EL efficiencies of individual Si solar cells in modules and arrays. The developed method enables the realization of quantitative open-circuit voltage mapping. [http://dx.doi.org/10.1063/1.4940159]

I. INTRODUCTION

Electroluminescence (EL) and photoluminescence (PL) imaging have been used to visualize failures in solar cells, such as electrode faults, cell cracks, ohmic contacts, shunts, and potential induced degradation.[1–10] More recently, PL and EL have also been developed as tools for the quantitative characterization of solar cell properties such as internal current-voltage (I-V) curves, internal radiative efficiencies, minority carrier lifetimes, diffusion lengths, and the series resistance.[11–21] The internal I-V analysis uses the so-called generalized Planck equation, which is based on the reciprocal relationship between EL and the solar cell external quantum efficiency (EQE).[11,14] Such characterizations are verified by measurements of the absolute EL intensity, which prevent us from making parametric adjustments or fittings even for series-connected arrays and multi-junction solar cells.[21] Because of these advantages, absolute luminescence imaging is applicable to quantitative mapping characterization of internal voltages and related properties of solar cells and arrays.

While calibration of the imaging camera is very important for absolute luminescence imaging, so far, calibration procedures and tools have not been developed for solar cell research. Reliable calibration standards are necessary because cooled imaging infrared cameras that enable sensitive detection of luminescence have been developed by many suppliers and the infrared camera technology is very frequently modified. Therefore, camera sensitivity may change depending on the sensor temperature and other conditions. An accurate, user-friendly, and readily available reference light source will enable easy calibration through the measurement of reference luminescence.

In this paper, we propose and demonstrate the use of a crystalline silicon (c-Si) solar cell as a secondary light-emitter standard for the calibration of the absolute sensitivity of a luminescence imaging camera. In Sec. II, we describe two measurement setups for determining the absolute EL rate of the Si solar cell. The first setup is based on a contact method using an InGaAs photodiode, and the second is based on an imaging method using an InGaAs camera. We calibrated the absolute sensitivity of these sensors considering the EL spectrum and angular distribution from the solar cell and the known spectral responses of the sensors. In Sec. III, we show the EL spectrum, angular distribution, quantitative image, and rates of the Si solar cell. The EL spectra remained unchanged with the injection current and the angular distribution followed Lambert's cosine law. We then acquired a quantitative EL image using the InGaAs camera. The obtained image agreed well with the injection-current distributions estimated using a simple model with parameters for lateral and vertical resistance, confirming the uniformity of the material quality and EL efficiency. The EL rates determined by the contact method agreed well with the integration of the quantitative image. In Sec. IV, we present an analysis of the relationship between the absolute EL rate and the solar cell EQE spectrum, and use the reciprocal relationship between the EL and solar cell operation to verify that the EL is consistent with the I-V characteristics under AM1.5G 1-sun illumination. In particular, the value of the open-circuit voltage $V_{oc} = 0.602 \pm 0.004$ V evaluated using EL agreed well with $V_{oc} = 0.598$ V measured using a solar simulator. This cell enables accurate and simple calibration of the absolute sensitivity of any type of camera that responds linearly to the EL from Si solar cells. The evaluations of the EL characteristics and the verification of their consistency with the I-V curves measured using the solar simulator establish the reliability of the I-V curves obtained from the absolute EL measurements by using the present cell as a standard emitter. In Sec. V, we discuss the calibration of arbitrary cameras using the proposed Si-solar-cell EL radiance standard, and in Sec. VI, we demonstrate the V_{oc} mapping of

a)Electronic mail: toshimitsu-mochiduki@aist.go.jp

a solar module using the measurements from absolute EL images. Finally, we discuss the advantages and future possible applications of the proposed method.

II. MATERIALS AND METHODS

In this study, we used a monocrystalline Si photovoltaic cell with a thickness of 180 μm and an area of 2.0 cm $\times$ 2.0 cm as the sample. As the substrate, we used boron-doped p-type Si with an n-doped layer that exhibits a sheet resistance of 60 $\Omega/\square$ formed by phosphorus diffusion into the top surface. An anti-reflection texture and a silicon-nitride passivation layer were formed on the top surface. The top surface has a busbar electrode with a thickness of 0.77 mm and a length of 17.5 mm near the edge, and eight finger electrodes with a thickness of 0.11 mm and length of 17.5 mm were connected to the busbar. The electrode coverage of the sample was $\eta_{\mathrm{cover}} = 0.072$.

We measured the I-V curve of the same sample under AM1.5G, 1-sun illumination using a WACOM WXS-163S-10 solar simulator. The short-circuit current was 134 mA, the open-circuit voltage was 0.598 V, and the energy conversion efficiency was 15.6%.

We measured the EQE of the cell using a Bunkoukeiki MSR-3 quantum efficiency measurement system. The excitation spot radius of the EQE measurement was 0.8 mm, and the spot was positioned at the cell center to ensure that the cell electrodes are avoided.

Figure 1 shows a schematic illustration of the setup of the EL measurements. To inject the current, we connected the sample cell to an Advantest R6240A DC current source. We measured the EL spectra using a 32-cm monochromator equipped with a 1024 pixel linear InGaAs photodiode array sensor and an optical fiber bundle for light collection. We acquired an EL image of the sample cell using a Xenics Xeva-320–1.7 InGaAs camera with thermoelectric cooling from a distance of 31 cm. The pixel format, focal length, and f-number of the InGaAs camera were 320 $\times$ 256, 35 mm, and 1.4, respectively. The exposure time varied from 10.8 to 100 ms, depending on the injection current. We also used this camera to measure the angular distribution of the radiation by rotating the sample cell. We independently measured the absolute rate of EL with (a) a contact method using an InGaAs photodiode (Hamamatsu Photonics G12181–030 K) with a radius of 3 mm, and (b) an imaging method using a Xenics InGaAs camera. To evaluate the absolute rate using the contact method, we placed the InGaAs photodiode parallel to the sample at a distance of 1 mm and measured the photocurrent. We obtained the EL image using the InGaAs camera, calibrated using lengthy but conventional procedures in the imaging method.

We measured the spectral response of the photodiode using MSR-3 with reference to the National Metrology Institute of Japan (NMIJ) traceable standard photodiode. The sensitivity of the photodiode was $\eta_{\mathrm{PD}} = 0.45$ A/W at the c-Si EL wavelength. We calibrated the InGaAs camera using the same NIMJ-traceable standard photodiode and a collimated light source with variable wavelengths, which was developed by ATTO Corp. We evaluated the sensitivity of the InGaAs camera sensor $\eta_{\mathrm{sensor}} = 1.24 \times 10^{-2}$ count/photon for the

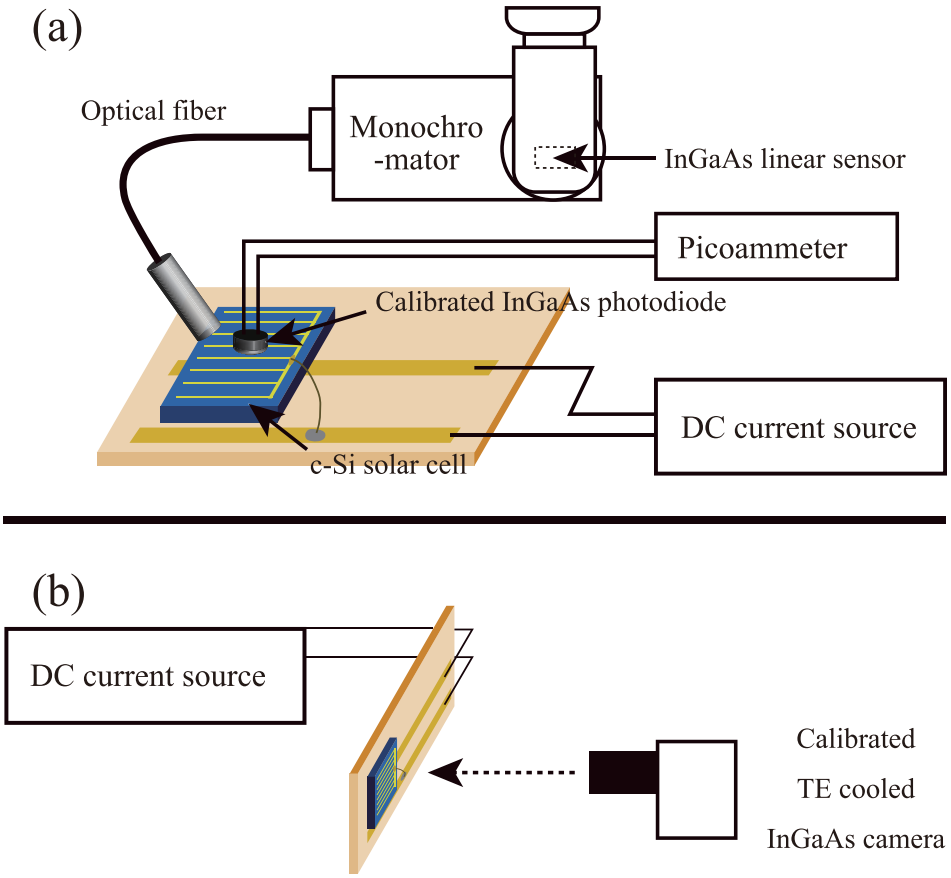

FIG. 1. (a) Schematic illustration of the setup used for the measurements of EL spectra with a monochromator and the absolute rate with an InGaAs photodiode. (b) EL imaging with an InGaAs camera.

incident light as an average of the products of the spectral response and the c-Si emission spectra. We calculated the collection efficiency of the camera for the cosine distribution of the EL and the solid angle of the camera aperture. The resulting efficiency of the camera lens was $\eta_{\text{lens}} = 1.62 \times 10^{-3}$ when the diameter of the entrance pupil was 25 mm and the distance between the sample and the camera lens was 31 cm. The absolute sensitivity of the camera for EL imaging was calculated as $\eta_{\text{camera}} = \eta_{\text{sensor}}\eta_{\text{lens}}t_{\text{exposure}} = 1.8 \times 10^{-7}$ count/(photon/s) for an exposure time $t_{\text{exposure}} = 10.8$ ms.

III. RESULTS

Figure 2 shows the EQE spectrum ϕ_{EQE}, the radiation spectrum ϕ_{rad}, and the EL spectrum ϕ_{EL} of the sample cell. The solid line in Fig. 2(a) shows ϕ_{EQE} and the dashed line shows the radiation spectrum $\phi_{\text{rad}} = \phi_{\text{EQE}}B_{300\text{K}}$ of the cell, where $B_{300\ \text{K}}$ is the blackbody spectrum at 300 K. Figure 2(b) shows the EL spectra of the cell for various injection currents represented by the three lower solid lines in Fig. 2(b), and with ϕ_{EQE} and ϕ_{rad} shown again at the top for comparison. While the EL intensity changed with the injection currents, the EL spectra were almost unchanged and were consistent with the radiation spectrum at 300 K. This consistency indicates that the solar cell was not heated by the injection currents and that the minority carriers were thermalized to the lattice temperature. This enables us to use the cell temperature $T = 300$ K in the subsequent analysis of the I-V curve.

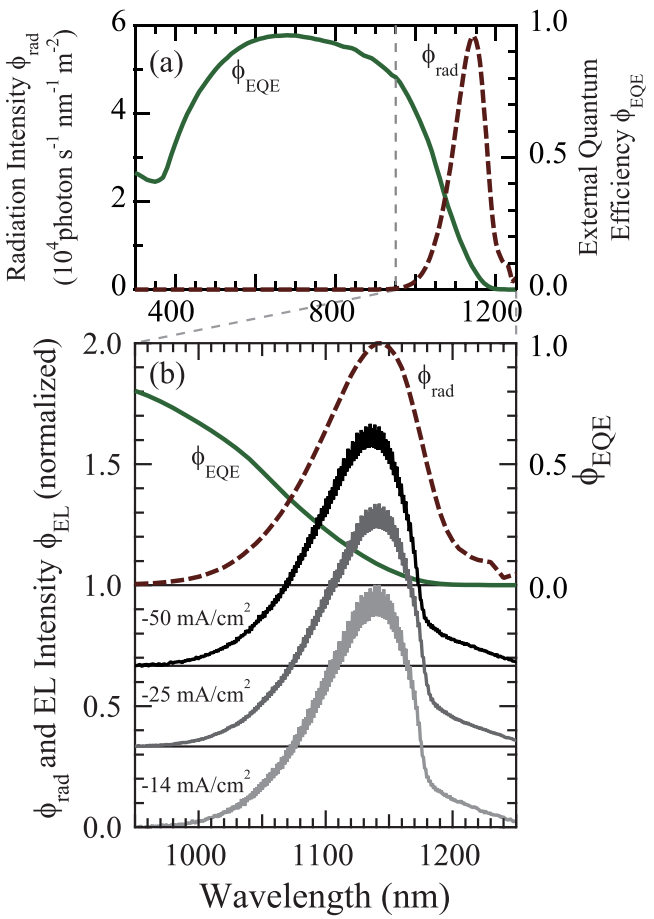

FIG. 2. (a) EQE and radiation spectra of the c-Si solar cell. (b) EL spectra of the sample with various injection currents. EQE and radiation spectra are shown again at the top for comparison.

Figure 3 shows the relative EL intensity of the sample cell for a forward current of 100 mA at various angles of incidence, θ_{cell}. Red circles show the observed intensity and dashed curves show the angle dependence proportional to $\cos(\theta_{\text{cell}})$. Inspection of the results in Fig. 3 shows that the sample cell follows Lambert's cosine law and that the radiance of the sample is constant for all observation angles.

Figure 4 shows the EL image of the sample for the forward current of 134 mA and exposure time of 10.8 ms, obtained using the InGaAs camera. By spatially integrating the image, we obtained an emission rate $R_{\text{ext}} = 2.85 \times 10^{13}$ s^{-1}. The EL efficiency of the sample was obtained using $\eta_{\text{ext}}^{\text{EL}} = \frac{eR_{\text{ext}}}{I_{\text{cell}}} = 3.40 \times 10^{-5}$.

The EL image also shows patterns along the electrodes, suggesting that the in-plane image of the spatial inhomogeneity of the injection current is due to the internal resistance of the sample. Assuming that the quality of the sample cell is homogeneous, for simplicity and clarity, we analyzed the EL inhomogeneity perpendicular to the finger electrodes in the 6.4 mm $< y <$ 19.2 mm range using a model similar to the 2D model used in the work of Nesswetter *et al.*[1] In this range, the EL image is nearly uniform along the y-axis and we assumed that x and y are variables that can be separated. Figure 5(a) shows the integrated EL intensity along the y-axis or the finger electrodes within the 6.4 mm $< y <$ 19.2 mm range. We then linearly interpolated the EL image for the integration. The red open circles and black dashed lines show the experimental results and the fitting curves to $j_h(x)$ in the model shown in Fig. 5(b), respectively. This model is the equivalent circuit of the sample and has been simplified to enable the analytical calculation of the spatial distribution of the injection current in order to describe the patterns in the image. Here, I_0, V_0, R_s, R_v, $I(x)$, $V(x)$, $j_h(x)$, W, and D are the injection current, voltage across the top and bottom electrodes, sheet resistance, differential resistance normal to the surface, current in the n-doped layer, local voltage in the n-doped layer, current density normal to the surface, width of the sample, and depth of the sample, respectively. Solving this model, we obtain

$$j_h(x) \propto \exp\{(x - L/2)\sqrt{R_s/R_vDW}\} + \exp\{-(x - L/2)\sqrt{R_s/R_vDW}\}, \quad (1)$$

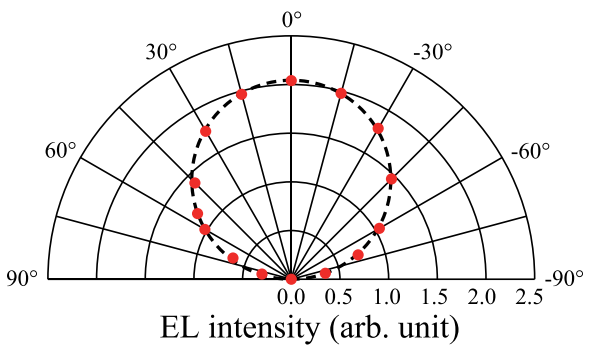

FIG. 3. Angular distribution of the EL intensity of the sample. Dashed line represents an ideal Lambertian radiator.

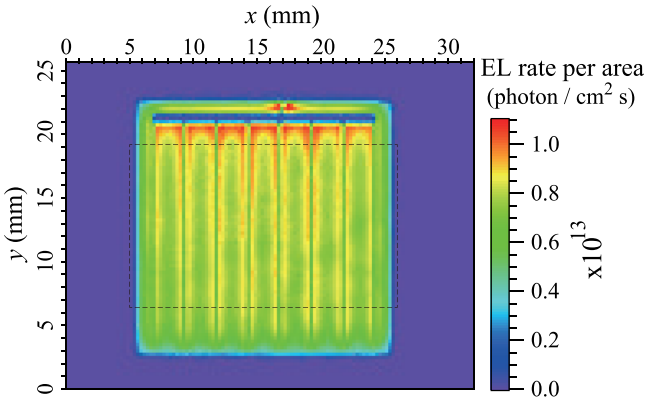

FIG. 4. Absolute EL image of the sample with injection current $I_{cell} = 134$ mA. Absolute EL rate of the entire sample is evaluated by spatial integration of the image. Dashed rectangle shows $6.4\,\text{mm} < y < 19.2\,\text{mm}$ area for which EL inhomogeneity is analyzed using the model shown in Fig. 5(b).

where L is the distance between the fingers, which is consistent with the integrated EL intensity between the finger electrodes with fitting parameters $R_s/R_v = 180$ and the EL intensity at each center between the electrodes. The results in Figs. 5(a) and 5(b) suggest that the EL efficiency of the solar cell is homogeneous and that the EL is spatially uniform when averaged over an area larger than the distance between the finger electrodes.

Figure 6 shows the absolute EL rate of the sample for various injection current values. The black dashed line and open circles in Fig. 6 show the EL emission rates R_{ext} measured independently by the imaging method and by the photodiode contact method, respectively. In the imaging method, we obtained R_{ext} by performing spatial integration of the absolute EL image. In the contact method, we evaluated the rate according to

$$R_{ext} = \frac{I_{PD}A}{\eta_{PD}E_{photon}A_{PD}}. \quad (2)$$

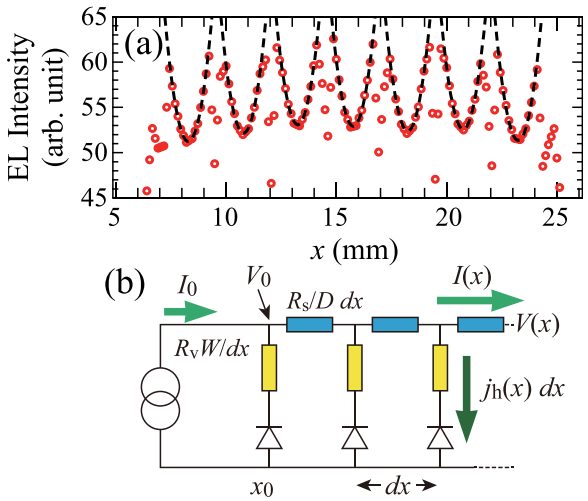

FIG. 5. (a) Integrated EL intensity along the finger electrodes shown by red circles and fitting curves based on the simulation shown as black dashed lines. (b) Simulation model that describes spatial in-plane inhomogeneity of the EL intensity.

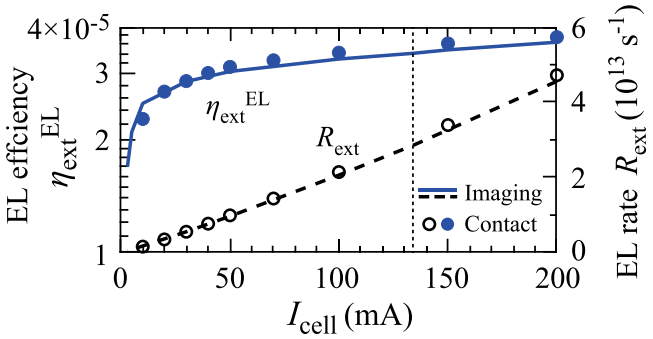

FIG. 6. EL rate and external efficiency of the cell for various injection currents, measured using the InGaAs camera and photodiode. The dashed dotted line indicates $I_{sc} = J_{sc}A = 134$ mA or the short-circuit current of the cell.

Here, $I_{PD}, A = 4.0\text{cm}^2, A_{PD} = 7.07 \times 10^{-2}\text{cm}^2, \eta_{PD} = 0.45\text{A/W}$, and $E_{photon} = 1.10\text{eV}$ are the signal current, surface area of the sample, surface area of the InGaAs photodiode, sensitivity of the photodiode, and average EL photon energy, respectively. The blue solid line and the filled circles in Fig. 6 represent the EL efficiency η_{ext}^{EL} determined using the camera and photodiode, respectively. We note that the agreement between these values confirms the accuracy of the measurements and the uniformity of the EL from the sample.

IV. VOLTAGE EVALUATION USING ABSOLUTE EL RATES

We evaluated the internal voltage of the solar cell obtained from the EQE spectrum and the absolute EL rate assuming a spatially homogeneous EL efficiency. The consistency between the model and the EL image in Fig. 5 supports the validity of this assumption. We determined the internal voltage V^{db} in the absence of non-radiative recombination of photoexcited carriers using the carrier balance equation, which is given as

$$J_{sc} - J = J_{rad}\exp(eV^{db}/k_BT). \quad (3)$$

This corresponds to the condition called the detailed-balance limit, which is also called the radiative limit or the Shockley-Queisser limit. In this analysis,

$$J_{sc} = \int_0^\infty dE\,\phi_{EQE}I_{sun}(1 - \eta_{cover}) = 33.4\,\text{mA cm}^{-2} \quad (4)$$

is the short-circuit current of the sample evaluated from the EQE spectrum, where I_{sun} is the solar emission spectrum under AM1.5 G solar conditions, and

$$J_{rad} = \int_0^\infty dE\,e\phi_{rad}(1 - \eta_{cover}) = 8.8 \times 10^{-14}\,\text{mA cm}^{-2} \quad (5)$$

is the radiation rate per unit area in terms of the current density. For non-radiative recombination, the internal voltage V^{EL} is given by

$$J_{sc} - J = \frac{J_{rad}\exp\left(eV^{EL}/k_BT\right)}{\eta_{ext}^{EL}} \quad (6)$$

without taking into account the series and shunt resistance. Hence, we obtain

$$V^{\mathrm{EL}} = V^{\mathrm{db}} + \frac{k_{\mathrm{B}}T}{e} \ln \eta_{\mathrm{ext}}^{\mathrm{EL}}. \tag{7}$$

Note that the values of $\eta_{\mathrm{ext}}^{\mathrm{EL}}$ in these equations are taken from Fig. 6 with the condition $J_{\mathrm{sc}} - J = I_{\mathrm{cell}}/A$. We used $\eta_{\mathrm{ext}}^{\mathrm{EL}}$ of the imaging method, which is the spatially averaged value measured with inhomogeneous current injection, to obtain a single V_{oc} value because $\eta_{\mathrm{ext}}^{\mathrm{EL}}$ is only weakly dependent on the injection density near $J = J_{\mathrm{sc}} = 33.4\,\mathrm{mA}$ or $I = 134\,\mathrm{mA}$, as shown in Fig. 6. In the absence of a large shunt resistance, the I-V characteristics of the cell can be reproduced by

$$V^{\mathrm{EL+R_s}} = V^{\mathrm{EL}} - JAR_{\mathrm{s}}, \tag{8}$$

where R_{s} is the series resistance of the cell.

Figure 7 shows the comparison between the I-V curves evaluated from $\eta_{\mathrm{ext}}^{\mathrm{EL}}$ measured with the imaging method using the carrier balance equations and an I-V curve measured with the solar simulator. The black open circles represent the results obtained from the solar simulator. The short-circuit current of $33.5\,\mathrm{mA/cm^2}$ measured using the solar simulator was very close to the value evaluated from the EQE. The open-circuit voltage is 0.598 V. The black dotted line and the yellow broken line show V^{db} and V^{EL}, respectively. The voltage difference between V^{db} and V^{EL} is due to non-radiative recombination, which is shown with blue stripes to the right and a dashed line to the left. V^{EL} at $J = 0$ gives an internal open-circuit voltage

$$\begin{aligned} V_{\mathrm{oc}} &= \frac{k_B T}{e} \left[\ln(J_{\mathrm{sc}}/J_{\mathrm{rad}}) + \ln \eta_{\mathrm{ext}}^{\mathrm{EL}}\right] \\ &= 0.8679 - 0.02585 \ln \eta_{\mathrm{ext}}^{\mathrm{EL}} = 0.6019\,\mathrm{V}. \end{aligned} \tag{9}$$

This value was close to that measured with the solar simulator.

The green solid line represents the I-V characteristics of the cell $V^{\mathrm{EL+R_s}} = V^{\mathrm{EL}} - I_{\mathrm{cell}} \times R_{\mathrm{s}}$ with series resistance $R_{\mathrm{s}} = 0.57\ \Omega$ and shows a good agreement with the I-V characteristics measured using the solar simulator. The voltage drop due to the series resistance JAR_{s} is shown in Fig. 7 with red stripes and a red dotted line.

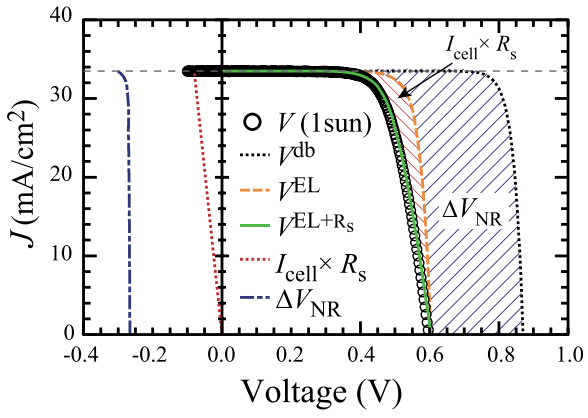

FIG. 7. I-V characteristics of the cell analyzed via EL and obtained using the solar simulator.

Based on our previous work,[22] we find that the calibrations of the present experiment have an uncertainty of ± 18% ($k = 2$), which corresponds to an uncertainty of ± 4.3 mV ($k = 2$) for the V_{oc} evaluation. This applies to the results in Fig. 7 and the evaluations for other solar cells using the camera calibrated in the proposed method. The values of V_{oc} obtained using EL and the solar simulator were within the range of the uncertainty.

The I-V characteristics of the solar cell were in agreement with the electrically measured I-L curve. This result shows that the measurement of the absolute EL rate enables an accurate evaluation of the internal voltage of Si solar cells without the use of a voltmeter or voltage probes.

V. Si-CELL LIGHT-EMISSION STANDARD FOR CAMERA CALIBRATION

In Secs. I–IV, we have shown that the absolute EL rates R_{ext} of the c-Si-cell sample obtained using the imaging and contact methods for various injection currents I_{cell} are consistent. The angular distribution of EL followed Lambert's cosine law and is proportional to $\cos(\theta_{\mathrm{cell}})$, and the in-plane distribution showed a homogeneous EL efficiency over the area $A = 2.0\,\mathrm{cm} \times 2.0\,\mathrm{cm}$. In short, the present c-Si-cell sample has an averaged absolute EL radiance $L_{\mathrm{cell}} = E_{\mathrm{photon}}(R_{\mathrm{ext}}/A)/\pi$ for all solid angles. Furthermore, we confirmed the agreement between the I-V curves evaluated using the absolute EL and measured using a voltmeter and a solar simulator. Note that the sample used in the present experiment is a typical mass-produced c-Si solar cell that is widely available commercially and displays high quality. The calibrations shown above are applicable to similar types of c-Si solar cells in a straightforward and simple manner.

Therefore, c-Si solar cells are suitable for use as secondary light-emission standards. In particular, such standards are useful for the calibration of the absolute sensitivity of infrared cameras used in absolute EL imaging for contactless V_{oc} mapping of various Si solar cells and arrays.

Figure 8(a) shows a schematic of the configuration for the camera calibration and the absolute EL imaging of a solar mini-module that includes 25 cells. For the camera calibration, we measured an EL image of the c-Si cell with a proper injection current I_{cell} as a secondary light-emission standard; this was then used to determine the camera sensitivity. For example, the present sample provided a Lambertian EL with an absolute rate per area of $R_{\mathrm{ext}}/A = 1.14 \times 10^{13}$ photon/s cm^2 for an injection current of $I_{\mathrm{cell}} = 200\,\mathrm{mA}$. The camera then detected an averaged intensity $C = 1713$ count/pixel for an exposure time of 10.8 ms. The distance r_{cell} between the standard cell and the camera was 4.2 m. In this case, we obtained a calibration factor $S = R_{\mathrm{ext}} t_{\mathrm{exposure}}/AC = 7.18 \times 10^7$ [photon/s cm^2]/[count/s pixel]. By measuring a sample solar module with the Lambertian emissivity in the same configuration, we can calculate the absolute EL rate per area of the module as the signal count

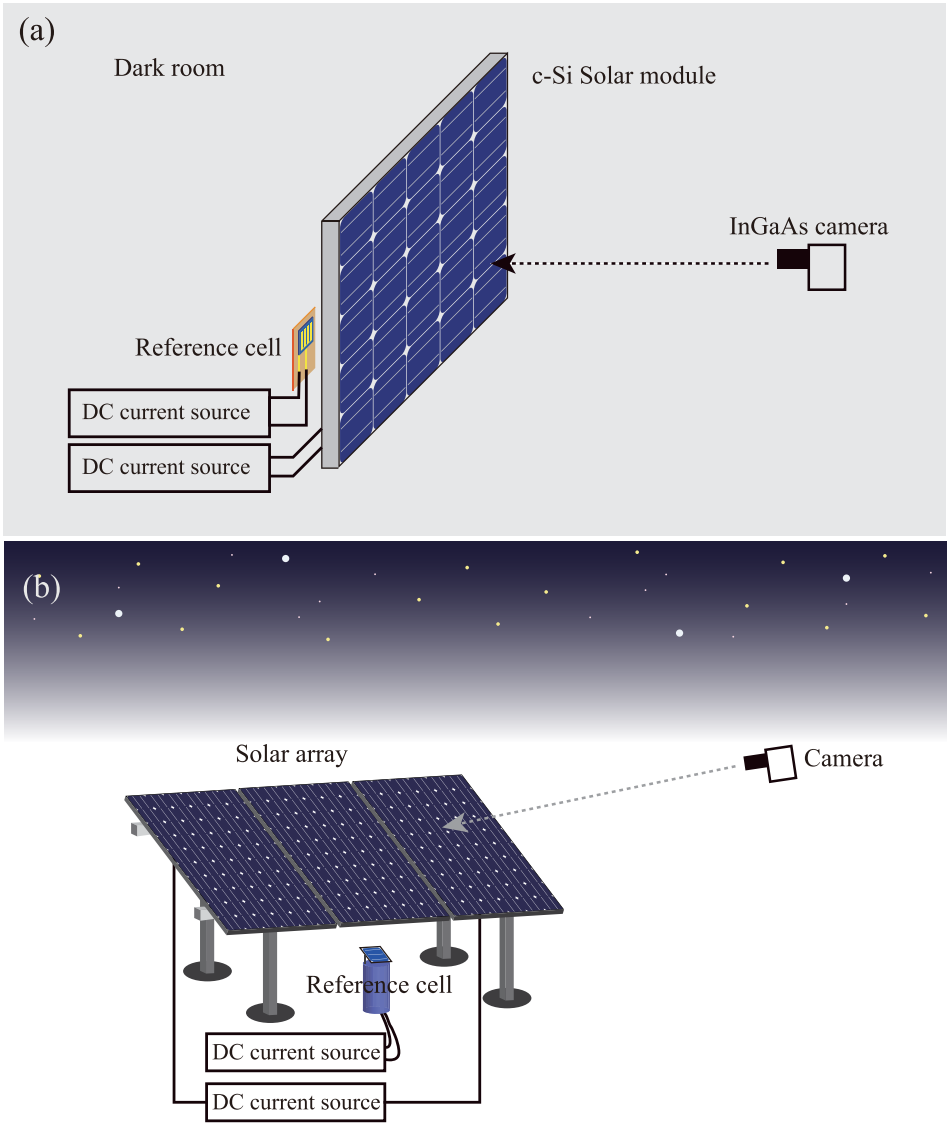

FIG. 8. (a) Schematic of absolute EL imaging of a solar module. (b) Schematic of an intended application of the proposed method. With appropriate shading or at night, the absolute EL image can be obtained outdoors using a camera and a standard light emitter.

per pixel per exposure time of the camera multiplied by the obtained calibration factor S; this is demonstrated in Sec. VI.

Note that the calibration factor S does not change with distance between the standard cell and the camera, r_{cell}, because both the cell image size and the detected light intensity are proportional to $1/r_{\text{cell}}^2$, and therefore, the changes in these two quantities cancel each other in the formula for C. Furthermore, the factor S does not change with the tilt angle θ_{cell} of the cell from the normal direction because both the image size and Lambert's emission intensity are proportional to $\cos(\theta_{\text{cell}})$, so that the changes in the image size and Lambert's emission intensity cancel each other in the formula for C. In other words, the apparent intensity C in count/pixel does not change with r_{cell} or θ_{cell}. These features are useful in the testing of solar arrays in power plants from a single camera position, as schematically shown in Fig. 8(b), where sensitivity calibrations are required for various values of r_{cell} and θ_{cell}. The absorption coefficient of air at the peak wavelength of EL from c-Si cells of 1.15 μm is as small as 1 km^{-1},[23] and should be considered only if the distance between the sample and the standard is much larger than 10 m. Otherwise, absorption by air can be neglected.

VI. ABSOLUTE EL IMAGING OF SOLAR MODULE FOR VOC MAPPING

Figure 9(a) shows the absolute EL image of the module measured in the configuration shown in Fig. 8(a) and calibrated to present R_{ext}/A using the method explained in Sec. V. The specifications of the sample module (Mitsubishi PV-MA1050KH) were as follows: open-circuit voltage of 15.6 V, short-circuit current of 8.90 A, and 25 cells with size of 15.6 cm × 15.6 cm. Thus, we set the injection current to 8.90 A for the module. As a reference, we placed the light-emitter-standard c-Si cell at the injection current of 200 mA next to the module sample, and the exposure time to 10.8 ms. The EL rate R_{ext} of each cell was obtained by the spatial integration of each cell image, and the external EL efficiency $\eta_{\text{ext}}^{\text{EL}} = \frac{eR_{\text{ext}}}{I_{\text{cell}}}$ was obtained.

Figure 9(b) shows the mapping of the open-circuit voltage V_{oc} of each cell, evaluated from the EL rates shown in Fig. 9(a). By using $J_{\text{rad}} = 8.8 \times 10^{-14}$ mA/cm^2 from the reference cell and $J_{\text{sc}} = 38.9$ mA/cm^2 from the measurement with a PVS 1116i solar simulator, we obtained the V_{oc} values using $V_{\text{oc}} = 0.8717 + 0.02585\ln(\eta_{\text{ext}}^{\text{EL}})$. The data shown in

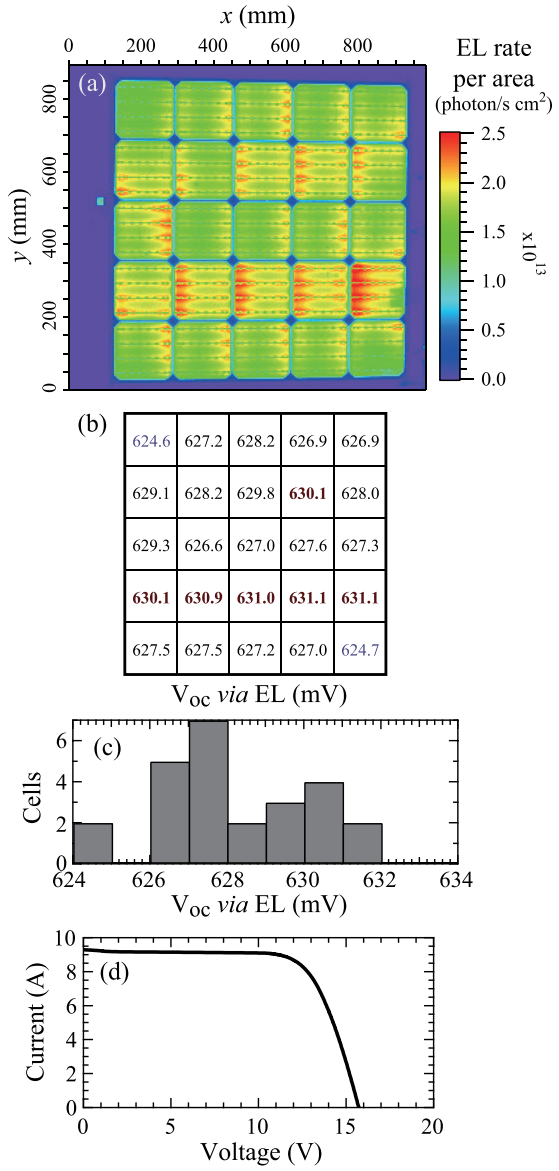

FIG. 9. (a) Absolute EL image of a c-Si solar module. (b) Mapping of the open-circuit voltage of cells enclosed within the module, evaluated with a procedure similar to that used for the data shown in Fig. 7. (c) Histogram of V_{oc} *via* EL shown in (b). (d) I-V characteristics of the module measured using PVS 1116i solar simulator.

Fig. 9(b) are the V_{oc} values of the cell at the corresponding positions in Fig. 9(a). The proposed method enables us to obtain a mapping of the V_{oc} of each cell using a single EL image. The averaged and total V_{oc} of all cells were 0.628 V and 15.71 V, respectively. Figure 9(c) shows the histogram of V_{oc} data obtained using EL. All of the evaluated V_{oc} values were between 0.624 V and 0.632 V, and the standard deviation of V_{oc} was 0.002 V, quantitatively indicating the good uniformity of the module.

Figure 9(d) shows the I-V curve of this module measured under AM1.5 G 1-sun illumination using a Nissinbo PVS1116i solar simulator. The I-V curve indicates that the effect of the shunt resistance on the V_{oc} is small. While the total series resistance can be derived from the obtained curve, the value of the resistance for each cell cannot be deduced from the available I-V data, preventing us from evaluating the entire I-V curve of each cell using the absolute EL rates. To obtain a single V_{oc} value following the procedure described in Sec. IV, we assumed that the effect of the series resistance on the evaluation of V_{oc} is small and the EL efficiency is uniform. The measured I-V curve gave a module $V_{oc} = 15.73$ V and an average cell $V_{oc} = 0.629$ V. These V_{oc} values agreed well with those derived using the absolute EL image, with the difference between the values lying within the ± 6.8 mV($k = 2$) uncertainty range.

Note that the uncertainty of the absolute EL efficiency measurement was 18%,[22] contributing 4.3 meV per cell to the uncertainty in the V_{oc} value obtained using $V_{oc} = V^{db} - (k_B T/e)\ln \eta_{ext}^{EL}$. The additional uncertainty in V_{oc} originates from J_{sc} and J_{rad} due to the dependence of V_{oc} on these quantities, as specified in the $V^{db} = (k_B T/e)\ln(J_{sc}/J_{rad})$ formula. The uncertainty in J_{sc} can be estimated as 6.3% from the difference between the specification value $J_{sc} = 36.6$ mA/cm^2 and the measured value $J_{sc} = 38.9$ mA/cm^2. Empirically, c-Si solar cells exhibit J_{sc} values between 32 and 40 mA/cm^2, so we may use the representative value of $J_{sc} = 36$ mA/cm^2 with an uncertainty of 10%, contributing 2.5 mV per cell to the uncertainty in the obtained V_{oc}. Because the band-edge absorption coefficient of the c-Si cell is almost constant, J_{rad} is mostly determined by the thickness, surface reflectivity, and transport properties, and we determine the estimated uncertainty to be 20%, which contributes further 4.7 mV per cell to the uncertainty in V_{oc}. From the square root of the squared sum of these uncertainty values, we estimate the uncertainty in the obtained V_{oc} as $\pm$ 6.8 mV($k = 2$) per cell or ± 0.17 V per module with 25 cells.

This result demonstrates that the values of V_{oc} for the cells in the modules can be evaluated using an absolute EL image obtained without contact, which is obtained quickly by a camera calibrated using the proposed light-emitter standard. We expect that the proposed method will be useful in studies of reliability of solar modules by quantitatively monitoring V_{oc} of the respective cells in the modules before and after installations, or during their use in power plants.

VII. SUMMARY

In summary, we demonstrated the use of a c-Si solar cell as a standard light source. The solar cell was a Lambertian radiator and the emission rate showed sufficient in-plane homogeneity. The absolute EL rate was consistently calibrated using both the imaging method and the contact method. The I-L profile of the cell was also consistent with the I-V curve measured with a solar simulator.

The presented method is a very useful tool for the evaluation of the internal I-V characteristics—particularly the open-circuit voltage V_{oc}—of Si solar cells and modules using the reciprocal relationship between EL and the solar cell operation. The proposed method enables us to evaluate V_{oc} using a simple setup without requiring the use of voltage probes or a solar simulator and can also be applied to the evaluation of solar cells in operational power plants.

ACKNOWLEDGMENTS

This work was partly supported by KAKENHI Nos. 26610081, 26390075, 15H03968, and 14F04907 from the Japan Society for the Promotion of Science (JSPS), the Photon Frontier Network Program of MEXT, JST-SENTAN, and JST-CREST in Japan.

[1]H. Nesswetter, W. Dyck, P. Lugli, A. W. Bett, and C. G. Zimmermann, J. Appl. Phys. **114**, 194510 (2013).
[2]P. Chaturvedi, B. Hoex, and T. M. Walsh, Sol. Energy Mater. Sol. Cells **108**, 78 (2013).
[3]S. Pingel, O. Frank, M. Winkler, S. Oaryan, T. Geipel, H. Hoehne, and J. Berghold, in *Conference Record of the IEEE Photovoltaic Specialists Conference* (PVSC, 2010), p. 2817.
[4]T. Fuyuki, H. Kondo, T. Yamazaki, Y. Takahashi, and Y. Uraoka, Appl. Phys. Lett. **86**, 262108 (2005).
[5]A. Kitiyanan, A. Ogane, A. Tani, T. Hatayama, H. Yano, Y. Uraoka, and T. Fuyuki, J. Appl. Phys. **106**, 043717 (2009).
[6]T. Kirchartz, A. Helbig, W. Reetz, M. Reuter, J. H. Werner, and U. Rau, Prog. Photovoltaics: Res. Appl. **17**, 394 (2009).
[7]M. Schneemann, T. Kirchartz, R. Carius, and U. Rau, J. Appl. Phys. **114**, 134509 (2013).
[8]M. D. Abbott, J. E. Cotter, F. W. Chen, T. Trupke, R. A. Bardos, and K. C. Fisher, J. Appl. Phys. **100**, 114514 (2006).
[9]A. Delamarre, L. Lombez, and J.-F. Guillemoles, Appl. Phys. Lett. **100**, 131108 (2012).
[10]A. Delamarre, L. Lombez, and J.-F. Guillemoles, J. Photonics Energy **2**, 027004 (2012).
[11]M. A. Green, J. Zhao, A. Wang, P. J. Reece, and M. Gal, Nature **412**, 805 (2001).
[12]D. Hinken, K. Ramspeck, K. Bothe, B. Fischer, and R. Brendel, Appl. Phys. Lett. **91**, 182104 (2007).
[13]T. Trupke, E. Pink, R. A. Bardos, and M. D. Abbott, Appl. Phys. Lett. **90**, 093506 (2007).
[14]U. Rau, Phys. Rev. B – Condens. Matter Mater. Phys. **76**, 085303 (2007).
[15]C. Shen, H. Kampwerth, M. Green, T. Trupke, J. Carstensen, and A. Schütt, Sol. Energy Mater. Sol. Cells **109**, 77 (2013).
[16]S. Roensch, R. Hoheisel, F. Dimroth, and A. W. Bett, Appl. Phys. Lett. **98**, 251113 (2011).
[17]R. Hoheisel, F. Dimroth, A. W. Bett, S. R. Messenger, P. P. Jenkins, and R. J. Walters, Sol. Energy Mater. Sol. Cells **108**, 235 (2013).
[18]J. F. Geisz, M. A. Steiner, I. García, S. R. Kurtz, and D. J. Friedman, Appl. Phys. Lett. **103**, 041118 (2013).
[19]A. Delamarre, M. Paire, J.-F. Guillemoles, and L. Lombez, Prog. Photovoltaics: Res. Appl. **23**, 1305 (2015).
[20]L. Zhu, C. Kim, M. Yoshita, S. Chen, S. Sato, T. Mochizuki, H. Akiyama, and Y. Kanemitsu, Appl. Phys. Lett. **104**, 031118 (2014).
[21]S. Chen, L. Zhu, M. Yoshita, T. Mochizuki, C. Kim, H. Akiyama, M. Imaizumi, and Y. Kanemitsu, Sci. Rep. **5**, 7836 (2015).
[22]M. Yoshita, L. Zhu, C. Kim, H. Akiyama, S. Chen, T. Mochizuki, H. Kubota, T. Nakamura, M. Imaizumi, and Y. Kanemitsu, in Proceedings of IEEE PVSC42 (PVSC, 2015).
[23]P. Sprangle, J. Peñano, A. Ting, and B. Hafizi, Naval Research Labs, 2004.